Genetic Ablation of cGMP-Dependent Protein Kinase Type I Causes Liver Inflammation and Fasting Hyperglycemia

Stefan Z. Lutz,[1] Anita M. Hennige,[1] Susanne Feil,[2] Andreas Peter,[1] Andrea Gerling,[2] Jürgen Machann,[3] Stefan M. Kröber,[4] Michaela Rath,[5] Annette Schürmann,[5] Cora Weigert,[1] Hans-Ulrich Häring,[1] and Robert Feil[2]

OBJECTIVE—The nitric oxide/cGMP/cGMP-dependent protein kinase type I (cGKI) signaling pathway regulates cell functions that play a pivotal role in the pathogenesis of type 2 diabetes. However, the impact of a dysfunction of this pathway for glucose metabolism in vivo is unknown.

RESEARCH DESIGN AND METHODS—The expression of cGKI in tissues relevant to insulin action was analyzed by immunohistochemistry. The metabolic consequences of a genetic deletion of cGKI were studied in mice that express cGKI selectively in smooth muscle but not in other cell types (cGKI-SM mice).

RESULTS—In wild-type mice, cGKI protein was detected in hepatic stellate cells, but not in hepatocytes, skeletal muscle, fat cells, or pancreatic β-cells. Compared with control animals, cGKI-SM mice had higher energy expenditure in the light phase associated with lower body weight and fat mass and increased insulin sensitivity. Mutant mice also showed higher fasting glucose levels, whereas insulin levels and intraperitoneal glucose tolerance test results were similar to those in control animals. Interleukin (IL)-6 signaling was strongly activated in the liver of cGKI-SM mice as demonstrated by increased levels of IL-6, phospho-signal transducer and activator of transcription 3 (Tyr 705), suppressor of cytokine signaling-3, and serum amyloid A2. Insulin-stimulated tyrosine phosphorylation of the insulin receptor in the liver was impaired in cGKI-SM mice. The fraction of Mac-2–positive macrophages in the liver was significantly higher in cGKI-SM mice than in control mice. In contrast with cGKI-SM mice, conditional knockout mice lacking cGKI only in the nervous system were normal with respect to body weight, energy expenditure, fasting glucose, IL-6, and insulin action in the liver.

CONCLUSIONS—Genetic deletion of cGKI in non-neuronal cells results in a complex metabolic phenotype, including liver inflammation and fasting hyperglycemia. Loss of cGKI in hepatic stellate cells may affect liver metabolism via a paracrine mechanism that involves enhanced macrophage infiltration and IL-6 signaling. *Diabetes* **60:1566–1576, 2011**

From the [1]Department of Internal Medicine, Division of Endocrinology, Diabetology, Vascular Disease, Nephrology and Clinical Chemistry, University of Tübingen, Tübingen, Germany; the [2]Interfakultäres Institut für Biochemie, University of Tübingen, Tübingen, Germany; the [3]Section on Experimental Radiology, Department of Diagnostic and Interventional Radiology, University of Tübingen, Tübingen, Germany; the [4]Institute of Pathology, University of Tübingen, Tübingen, Germany; and the [5]Department of Experimental Diabetology, German Institute of Human Nutrition, Potsdam-Rehbruecke, Nuthetal, Germany.

Corresponding author: Hans-Ulrich Häring, hans-ulrich.haering@med.uni-tuebingen.de.

Received 7 July 2010 and accepted 22 February 2011.

DOI: 10.2337/db10-0760

This article contains Supplementary Data online at http://diabetes.diabetesjournals.org/lookup/suppl/doi:10.2337/db10-0760/-/DC1.

H-.U.H. and R.F. contributed equally to this study.

The nitric oxide (NO)/cGMP pathway modulates cell functions in tissues that play a pivotal role in the pathogenesis of type 2 diabetes (1,2). One important effector of cGMP is the serine/threonine kinase cGMP-dependent protein kinase type I (cGKI) (3,4). cGKI exists in two isoforms, cGKIα and cGKIβ, which are transcribed from the *prkg1* gene and differ only in their *N*-terminal region (~100 residues). Both isoforms are widely distributed in eukaryotes and regulate important functions of the cardiovascular and nervous system (5–7). However, it is not well understood whether cGMP/cGKI signaling does affect insulin action in peripheral tissues or the brain. Although a modulation of β-cell apoptosis via cGMP is well accepted (8), the role of NO and cGMP in the stimulation of insulin secretion is controversially discussed (1,2). The involvement of cGKI as a potential cGMP effector in these processes and its impact on insulin-sensitive tissues like liver and skeletal muscle are not clear. Miyashita et al. (9) recently reported the metabolic characterization of a cGKI transgenic mouse line. The overexpression of cGKI attenuated diet-induced obesity and insulin resistance. Moreover, cGKI transgenic mice were lean and showed increased insulin sensitivity. However, the consequences of a genetic deletion of the endogenous cGKI for metabolic regulation and inflammation have not been investigated yet.

In the current study, a potential interaction between the cGMP/cGKI and the insulin signaling pathway was analyzed in mice that express cGKI selectively in smooth muscle to obtain a viable phenotype but not in other cell types (cGKI-SM mice). In addition to a detailed in vivo characterization of metabolic parameters, mice were injected with human insulin, insulin receptor (IR) phosphorylation was monitored in liver and skeletal muscle, and the inflammatory status on deletion of cGKI was analyzed. Our data suggest that cGKI action is crucial for an adequate liver metabolism, because a loss of this kinase results in a metabolic phenotype that is associated with liver inflammation and fasting hyperglycemia.

RESEARCH DESIGN AND METHODS

Experimental animals. The generation of cGKI smooth muscle rescue (cGKI-SM) mice has been described (10). cGKI-SM mice are deficient for endogenous cGKI ($cGKI^{L-/L-}$) and express the cGKIα or the cGKIβ isoform under the control of the smooth muscle-specific SM22α promoter (SM-Iα or SM-Iβ rescue, respectively). Six- to nine-month-old male SM-Iα rescue or SM-Iβ rescue mice on a 129/Sv genetic background (genotype: $cGKI^{L-/L-}$;$SM\text{-}I\alpha^{+/-}$ or $cGKI^{L-/L-}$;$SM\text{-}I\beta^{+/-}$) were compared with litter-matched control mice that expressed both endogenous cGKI and the smooth muscle rescue transgene (genotype:

cGKI$^{+/L}$;SM-Iα$^{+/-}$ or cGKI$^{+/L}$;SM-Iβ$^{+/-}$, collectively referred to as "control" in the text). Because we could not detect any difference between SM-Iα and SM-Iβ rescue mice in terms of glucose homeostasis, we use the denotation "cGKI-SM" with regard to both groups. The specific function of cGKI in the nervous system was studied in 5- to 12-month-old male neuron-specific knockout mice (cGKI-BKO mice) on a C57BL/6 genetic background (genotype: cGKI$^{L/L2}$;Nes-Cre$^{tg/0}$) generated via Cre/loxP recombination by crossing a loxP-flanked cGKI mouse line with Nestin-Cre mice as described (11). They were compared with litter-matched control mice (genotype: cGKI$^{+/L2}$;Nes-Cre$^{tg/0}$). Mice were kept on a 12-h/12-h light/dark cycle (lights on at 6:00 A.M.) and had access to a regular chow ad libitum. All procedures were conducted according to the guidelines of laboratory animal care and were approved by the local governmental commission for animal research.

Immunohistochemistry and Western blot analysis. For immunohistochemistry, animals were deeply anesthetized and perfused with 10% phosphate-buffered formalin. Tissues were dissected and postfixed for 2 h in PBS containing 2% formaldehyde and 0.2% glutaraldehyde, embedded in paraffin, and cut at 10 μm. Sections were stained with the rabbit polyclonal cGKI common (DH) antibody (1:1,500) (12), a rabbit polyclonal cellular retinol binding protein (CRBP)-I antibody (1:200, sc-30106, Santa Cruz Biotechnology, Santa Cruz, CA), or a rat monoclonal Mac-2 antibody (1:200, CL8942AP, Cedarlane, Ontario, Canada). For detection of primary antibodies, the avidin-biotin method with 3,3′ diaminobenzidine tetrahydrochloride or Vector Blue substrate as a chromogen was used (Vector Laboratories, Burlingame, CA). To control for the specificity of cGKI immunostainings, tissues derived from 3- to 6-week-old mice with a global deletion of cGKI (cGKI$^{L/L}$) (13) were used. To determine the fraction of CRBP-I or Mac-2–positive cells, nuclei were stained by incubation of the sections in PBS containing 1 μg/mL Hoechst No. 33258 (Sigma, München, Germany) for 10 min and counted at 100× magnification.

Western blot analysis of tissue lysates was done with antibodies against phospho-Akt (Ser473), phospho-signal transducer and activator of transcription 3 (STAT3) (Tyr705), and GAPDH (9271, 9131, and 2118, respectively, Cell Signaling Technology, Beverly, MA) against phosphoenolpyruvate carboxykinase (PEPCK) (sc-32879, Santa Cruz, Heidelberg, Germany) and suppressor of cytokine signaling (SOCS)-3 (L210, Cell Signaling Technology). Signals were visualized with an enhanced chemiluminescence system (Amersham Biosciences, Buckinghamshire, U.K.). For the analysis of PEPCK and glucose-6-phosphatase, mice were fasted for 16 h and then refed for 6 h.

Analysis of body fat. Intraabdominal fat pads were dissected, and their wet weight was determined. Magnetic resonance imaging analysis of fat volume was done in anesthetized mice on a 3-T whole-body magnetic resonance system (Magnetom Trio, Siemens Healthcare, Erlangen, Germany) applying a T1-weighted fast spin-echo technique. Mice were placed in a prone position in the wrist coil of the system. Images were recorded with an in-plane spatial resolution of 0.25 mm and a slice thickness of 2 mm. Postprocessing was done as described (14).

Liver tissue was fixed in 4% paraformaldehyde in PBS for the histologic detection of liver fat. Hematoxylin–eosin staining of paraffin liver sections was carried out for analysis of fat content by visual inspection of vesicles.

To determine the hepatic triglyceride content, livers were homogenized in PBS containing 1% Triton X-100 using a TissueLyser (QIAGEN Sciences, Germantown, MD). Triglycerides of liver homogenates were quantified using the ADVIA 1650 clinical chemistry analyzer (Siemens Healthcare Diagnostics, Eschborn, Germany).

Measurement of food intake, locomotor activity, and energy expenditure. Mice were habituated to the test cages for 2 days before trials, and the measurement period lasted 5–6 days. Food intake was recorded with an automated drinking and feeding monitor system (TSE Systems GmbH, Bad Homburg, Germany), consisting of Macrolon type III cages equipped with baskets connected to weight sensors. The baskets contained diet pellets and were freely accessible to the mice. Locomotor activity was recorded with an automated infrared motion sensor attached to the Macrolon type III cage lid (TSE Systems GmbH). The sensor monitors the activity of one mouse by sensing the body-heat image. The software records the total counts during a measuring time interval. Thereby, the data provide a relative measure of the duration and intensity of the activity of the mice.

Total energy expenditure (TEE) was measured by indirect calorimetry at 22°C for 24 h with an open circuitry calorimetry system (TSE, Bad Homburg, Germany) as described previously (15). Before recoding the rate of oxygen consumption (VO_2) and the rate of carbon dioxide production (VCO_2), mice were allowed to adapt to the Macrolon type II cage and to the system for 2 days. The airtight respiratory cages were measured with a flow rate of ~0.38 L/min. VO_2 and VCO_2 were recorded for 1.5 min in 16-min intervals for each animal, so that three or four data points were obtained every other hour. TEE (kcal × h^{-1}) was calculated with the equation TEE = 16.17 × VO_2 + 5.03 × VCO_2 − 5.98 × N, where N is excreted nitrogen and was assumed to be (0.1 g × d^{-1}). Metabolic body mass-specific TEE was calculated by dividing TEE (kcal × h^{-1}) by body weight$^{0.75}$ of the animal and expressed as (kcal × h^{-1} × kg^{-1}).

Analysis of blood samples. Glucose levels were sampled from tail bleeds using a Glucometer Elite (Bayer, Elkhart, IN). Serum insulin and fasting serum adiponectin were determined by a radioimmunoassay (Linco Research, St. Charles, MO), and interleukin (IL)-6 concentrations were measured by the Quantikine Immunoassay (R&D Systems, Minneapolis, MN). Mouse inflammatory cytokines were screened by using a Multi-Analyte ELISArray Kit (MEM-004A, SABiosciences, Frederick, MD). Nonesterified fatty acids (NEFAs) were measured in the EDTA-plasma collected after decapitation. NEFA concentrations were detected using an enzymatic method (WAKO Chemicals, Neuss, Germany) on the automated clinical chemistry analyzer ADVIA 1800 (Siemens Healthcare Diagnostics).

Analysis of glucose homeostasis and insulin sensitivity. For the glucose tolerance test, mice were fasted overnight and 2 g/kg body wt α-D-glucose was injected intraperitoneally. To determine insulin sensitivity, mice received 0.75 units/kg body wt insulin intraperitoneally (Actrapid, Novo Nordisk, Denmark). To measure glucose-stimulated insulin release, mice were injected after an overnight fast with 3 g/kg body wt α-D-glucose.

In vivo insulin stimulation and IR phosphorylation. After an overnight fast, anesthetized mice were injected into the inferior vena cava with 2 units of human insulin. After 7 min, liver and skeletal muscle tissues were dissected and lysed at 4°C in 20 mmol/L Tris (pH 7,4) containing 2 mmol/L EDTA, 137 mmol/L NaCl, 1% NP-40, 10% glycerol, 12 mmol/L β-glycerol phosphate, 1 mmol/L phenylmethylsulfonyl fluoride, and 10 μg/mL leupeptin and aprotinin. Homogenates were incubated for 30 min on ice and then clarified by centrifugation at 12,000*g* for 20 min at 4°C. Supernatants (500 μg of total protein) were immunoprecipitated with antibodies directed against the carboxy terminus of the IR (KKNGRILTLPRSNPS; a gift from R. Lammers, University of Tübingen, Germany). Immunocomplexes were then resolved by SDS-PAGE and immunoblotted with antiphosphotyrosine antibody (PY20; Santa Cruz Biotechnology, Santa Cruz, CA). Signals were visualized with an enhanced chemiluminescence system (Amersham Biosciences, Buckinghamshire, U.K.), and densitometric analysis was performed with software from Herolab GmbH (Wiesloch, Germany).

Gene expression analysis. For mRNA measurements, tissues were frozen in liquid nitrogen. Total RNA was isolated with QIAzol lysis reagent (QIAGEN Sciences, Germantown, MD).The RNA was cleaned up with RNeasy Mini Kit (QIAGEN GmbH, Hilden, Germany), treated with RNase-free DNase I, and transcribed into cDNA using the first-strand cDNA kit from Roche Diagnostics

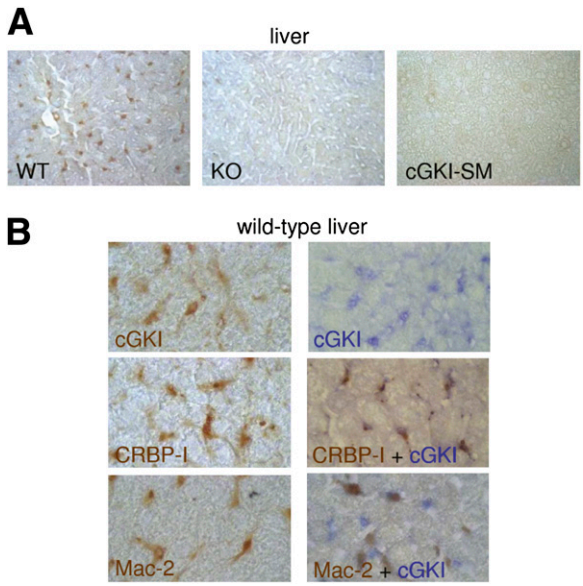

FIG. 1. Immunohistochemical analysis of cGKI expression in the liver of WT, global cGKI KO, and cGKI-SM mice. *A*: Liver sections were stained with an antibody against cGKI. *B*: Immunohistochemical single and double stainings of WT liver for cGKI (*upper left panel* in brown; *all right panels* in blue), CRBP-I (*middle panels* in brown), and Mac-2 (*lower panels* in brown). Original magnifications were 40× (*A*) and 100× (*B*). For each genotype, at least four mice were analyzed. Photomicrographs are representative of one to three stained sections per mouse. (A high-quality digital representation of this figure is available in the online issue.)

(Mannheim, Germany). Quantitative PCR was performed with SYBR Green I dye on a high-speed thermal cycler with integrated microvolume fluorometer (Roche Diagnostics). Primers were obtained from Invitrogen (Karlsruhe, Germany). Primer sequences can be provided on request. Measurements were performed in duplicate. RNA content was normalized to β-actin RNA and is given in relative expression.

Statistical analysis. Data are expressed as mean ± SEM, and the numbers of independent experiments or mice are indicated in Figs. 1–8. For statistical analysis, the groups were compared using the unpaired Student *t* test, if not stated otherwise. The level of significance adopted was $P < 0.05$ ($^{*}P < 0.05$, $^{**}P < 0.01$, $^{***}P < 0.001$, or n.s., not significant). The statistical software package JMP 7.0 (SAS Institute Inc., Cary, NC) was used.

RESULTS

Expression of cGKI in insulin-sensitive tissues. Previous work has shown that the cGKI is strongly expressed in several brain regions that also contain high concentrations of the IR, such as the hypothalamus, cerebellum, and hippocampus (16,17). However, the presence of cGKI in peripheral insulin-sensitive tissues has not been investigated in detail. Thus, the expression pattern of cGKI was determined in insulin-sensitive tissues of wild-type mice. By immunohistochemical staining, the cGKI protein was not detected in fat cells of white or brown adipose tissue or in skeletal muscle, pancreatic β-cells, or kidney epithelial cells (data not shown). In liver sections, hepatocytes were clearly negative for cGKI, but a fraction of non-hepatocytes was strongly immunopositive (Fig. 1*A*). Notably, these signals were specific for cGKI because they were not observed in liver sections of cGKI knockout mice. Moreover, the cGKI signals were also absent in the liver of cGKI-SM mice. The latter finding suggested that the cGKI-positive liver cells are not smooth muscle cells and that the cGKI-SM mouse model can be used to study the effect of cGKI deletion in these cells. To characterize the cGKI-positive cells in the liver, sections were stained with antibodies against CRBP-I, a marker for hepatic stellate cells (18), and Mac-2, which is expressed in liver macrophages (19). These analyses indicated that cGKI expression in the liver is confined to CRBP-I–positive hepatic stellate cells but not to Mac-2–positive macrophages (Fig. 1*B*).

To study the metabolic effects of cGKI deletion, conventional knockout mice are not useful because most of them die before 6 weeks of age as the result of smooth

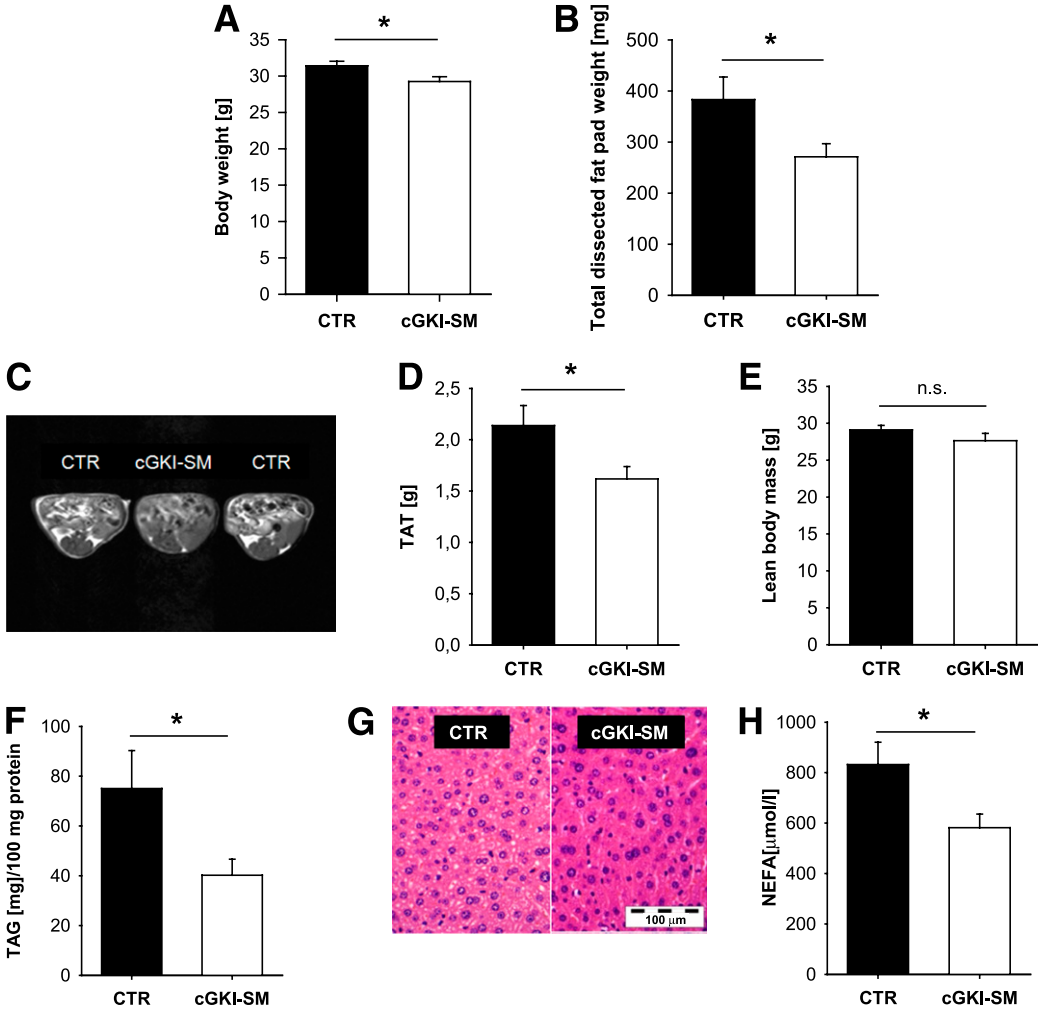

FIG. 2. Body weight and fat distribution in cGKI-SM (open bars) and control (black bars) mice that were fed a chow diet. *A*: Body weight of cGKI-SM ($n = 16$) and control ($n = 12$) mice. *B*: Dissected fat pad weight in cGKI-SM and control mice ($n = 11$ per group). *C*: Magnetic resonance imaging analysis of visceral and subcutaneous fat deposits: total adipose tissue (*D*) and lean body mass (*E*) ($n = 6$ mice per group). *F*: Liver triacylglycerol content ($n = 3$–6 mice per group). *G*: Hematoxylin–eosin staining of liver sections. Images are representative of eight stained sections per group ($n = 8$ mice per group). *H*: NEFAs in plasma of cGKI-SM and control mice ($n = 11$ mice per group). CTR, control; TAG, triacylglycerol; TAT, total adipose tissue. (A high-quality digital representation of this figure is available in the online issue.)

muscle dysfunction (10,20). Therefore, in the current study two conditional cGKI-deficient mouse models were used: cGKI smooth muscle rescue mice that express cGKI selectively in smooth muscle but not in other cell types (cGKI-SM mice) (10) and neuron-specific knockout mice lacking cGKI in the brain (cGKI-BKO mice) (11). In contrast with cGKI null mutants, cGKI-SM mice and cGKI-BKO mice have an almost normal life span (10,11,20).

cGKI-SM mice exhibit reduced adipose tissue, liver fat, and NEFAs. The impact of cGKI ablation on energy metabolism was examined in cGKI-SM mice and litter-matched control mice that were fed a standard diet. Compared with controls, cGKI-SM mice displayed lower body weight (Fig. 2*A*) that was associated with a significantly decreased fat pad weight (Fig. 2*B*). As measured by magnetic resonance imaging, cGKI-SM mice had less total adipose tissue (Fig. 2*C* and *D*), whereas their lean body mass was similar to that of control mice (Fig. 2*E*). In line with their lean phenotype, cGKI-SM mice had a lower hepatic triacylglycerol content (Fig. 2*F*) associated with a decrease in the size and number of liver fat droplets (Fig. 2*G*). Moreover, cGKI-SM mice had less circulating NEFAs in their plasma compared with controls (Fig. 2*H*).

cGKI-SM mice show higher energy expenditure in the light phase. cGKI-SM mice appeared normal with respect to food intake (Fig. 3*A*) and general locomotor activity (Fig. 3*B*), both during the light and dark phases. In addition, we determined energy expenditure of cGKI-SM and control mice over a 24-h period. Although no difference could be detected in the dark phase, cGKI-SM mice displayed significantly elevated energy expenditure in the light phase compared with control mice (Fig. 3*C*).

Elevated fasting blood glucose levels despite improved insulin sensitivity and unaltered glucose tolerance and insulin levels in cGKI-SM mice. Although there was no difference in blood glucose levels in the fed state, fasting blood glucose levels were significantly increased in cGKI-SM mice compared with control mice (Fig. 4*A* and *B*). In a glucose tolerance test, no difference in blood glucose levels was detectable between cGKI-SM and control mice (Fig. 4*C*). The glucose disappearance rate in an insulin tolerance test was higher in cGKI-SM than in control mice (Fig. 4*D*). After intraperitoneal administration of a high dose of glucose, no difference in glucose-stimulated insulin release was detectable between cGKI-SM and control mice (Fig. 4*E*). Taken together, cGKI-SM mice displayed unaltered glucose tolerance and normal basal and glucose-stimulated insulin release. However, these mouse mutants showed improved insulin sensitivity and increased fasting glucose levels.

Insulin action is not affected in muscle but impaired in the liver of cGKI-SM mice. In vivo, insulin action was assessed after intravenous insulin application. In skeletal muscle, intravenous injection of insulin led to a slightly stronger increase in tyrosine phosphorylation of the IR in cGKI-SM mice than in control mice, but this difference did not reach statistical significance (Fig. 5*A* and *B*). In the liver of cGKI-SM mice, basal and insulin-induced tyrosine phosphorylation of the IR was significantly decreased (Fig. 5*C* and *D*). Moreover, liver tissue of cGKI-SM mice displayed reduced Akt phosphorylation at Ser473 on insulin stimulation (Fig. 5*C* and *D*). These findings favored the idea that cGKI-SM mice show normal insulin action in skeletal muscle but insulin resistance in the liver. Indeed, expression of PEPCK, which catalyzes a rate-limiting step of gluconeogenesis, was significantly increased in the liver

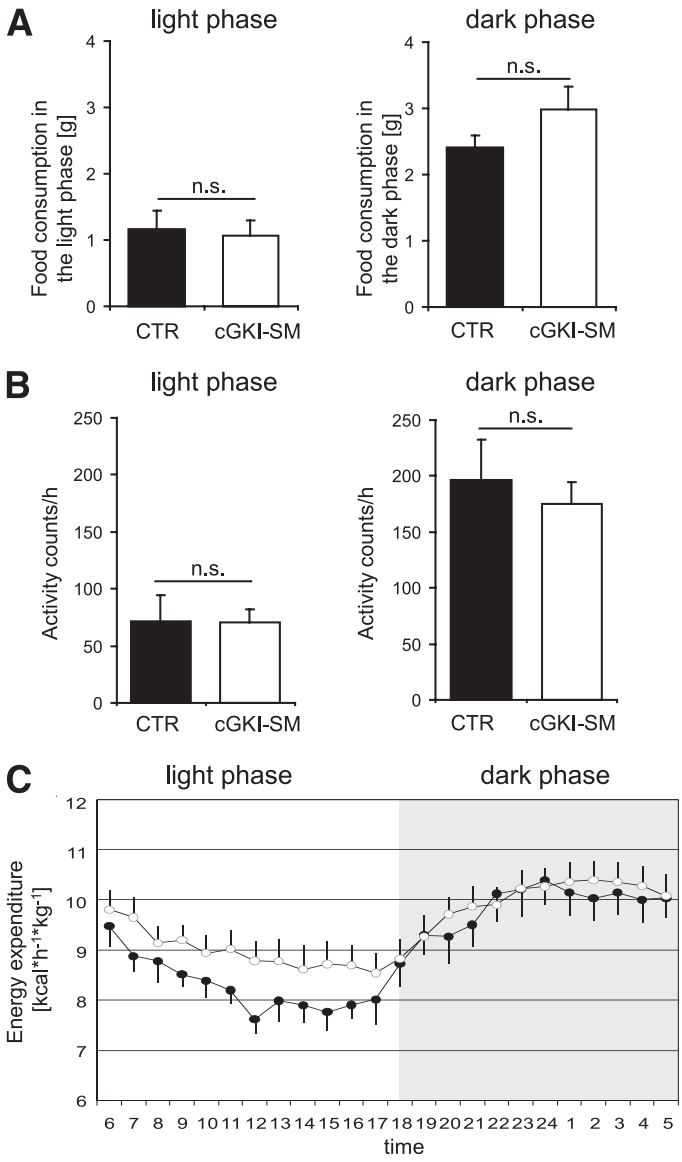

FIG. 3. Food intake (*A*), general locomotor activity (*B*), and total energy expenditure (*C*) were monitored over 24 h in cGKI-SM mice (open bars and symbols, $n = 10$) and control mice (black bars and symbols, $n = 6$) as described in RESEARCH DESIGN AND METHODS. Animals were analyzed for 5–6 days. Data shown were obtained from day 4 and are representative of the whole measurement period. Total energy expenditure is expressed in kilocalories per hour and metabolic body mass (kcal × h^{-1} × kg^{-1}). During the light phase, the cGKI-SM mice showed significantly higher energy expenditure than control mice ($P < 0.001$, two-way ANOVA). CTR, control.

of cGKI-SM mice after fasting and refeeding (Fig. 5*E*). However, the reduced IR phosphorylation in the liver of cGKI-SM mice did not result in significant changes of hepatic glycogen content or expression of glucose-6-phosphatase mRNA (Supplementary Fig. 1*A* and *B*).

In hepatic insulin resistance, liver-specific fetuin-A can be upregulated, leading to low-grade inflammation and hypoadiponectinemia (21). Indeed, fetuin-A mRNA was clearly elevated in the liver of cGKI-SM mice (Fig. 5*F*), whereas circulating adiponectin levels were lower (Fig. 5*G*).

The IL-6 signaling cascade is strongly activated in the liver of cGKI-SM mice. In parallel to the impaired insulin action in the liver, a marked increase of IL-6 mRNA was observed in liver tissue of cGKI-SM mice (Fig. 6*A*) associated with significantly elevated circulating IL-6 levels

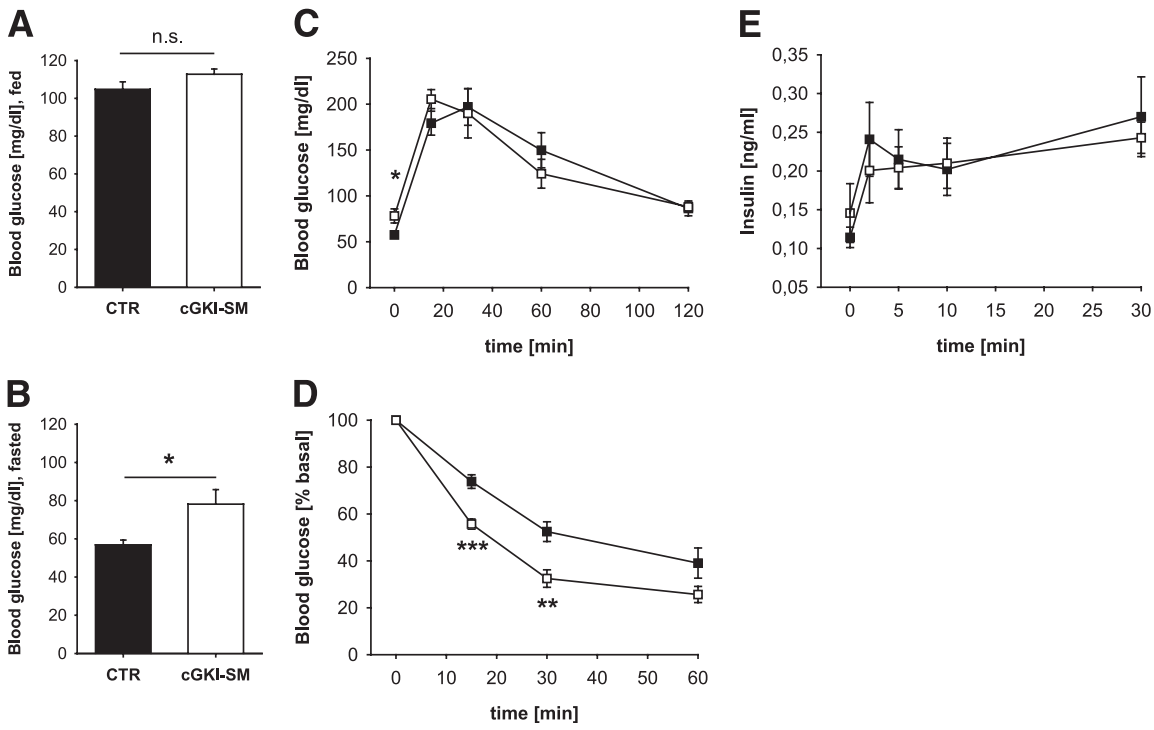

FIG. 4. Glucose homeostasis and insulin sensitivity in cGKI-SM (open bars and symbols) and control (black bars and symbols) mice. Blood glucose concentrations were measured in tail blood of mice fed ad libitum (*A*) and mice fasted overnight (*B*) (n = 7–15 mice per group). *C*: Glucose tolerance tests were performed in overnight fasted mice after intraperitoneal loading with 2 g α-D-glucose per kg body wt. Tail blood samples were taken at the indicated time points, and glucose was determined (n = 7–8 mice per group). *D*: Insulin tolerance tests were performed in fed mice after intraperitoneal loading with 0.75 units of human insulin per kg body wt. Tail blood samples were taken at the indicated time points, and glucose was determined (n = 7–8 mice per group). *E*: Glucose-stimulated insulin release. Mice fasted overnight were injected intraperitoneally with α-D-glucose (3 g/kg body wt), and serum insulin concentrations were measured at the indicated time points (n = 7 mice per group). CTR, control.

(Fig. 6*B*). Of note, elevated IL-6 mRNA expression seemed to be restricted to the liver because skeletal muscle, white adipose tissue, and spleen of cGKI-SM mice showed no significant alterations (Fig. 6*A*). Furthermore, gene expression analysis of tumor necrosis factor-α (Supplementary Fig. 1*C*), another proinflammatory protein, revealed no upregulation in the liver of cGKI-SM mice, and other proinflammatory cytokines (IL-2, IL-4, IL-10, IL-12, IL-17A, interferon-γ) were undetectable in the serum of cGKI-SM mice (data not shown). These results, together with the previous finding that the spleens of cGKI-SM mice do not show altered levels of T cells, B cells, and cytokines (22), indicated that the cGKI-SM mice studied did not have systemic inflammation.

Because cGKI-SM mice showed elevated IL-6 levels, we monitored the activity of the IL-6 signaling pathway in the liver of mutant and control mice. Several studies have reported enhanced hepatic STAT3 activation due to IL-6 action (23–25), so we first analyzed the phosphorylation status of the IL-6 mediator STAT3 and then the expression of IL-6–regulated genes. In line with an activation of the IL-6 signaling pathway, phosphorylation of hepatic STAT3 at tyrosine 705, which is known to be phosphorylated on IL-6 stimulation (26), was stronger in cGKI-SM mice than in control mice (Fig. 6*C*). An important effector of IL-6 is the SOCS-3. It has been shown that IL-6 induces SOCS-3 expression in hepatocytes leading to inhibition of the insulin signaling cascade (27). Indeed, SOCS-3 mRNA levels were increased approximately fivefold in liver tissue of cGKI-SM mice compared with controls (Fig. 6*D*). The mRNA level of serum amyloid A2, another IL-6/STAT3–regulated gene (28), was ~11-fold higher in the liver of cGKI-SM mice than in controls (Fig. 6*E*). Taken together, these data indicated that cGKI-SM mice display an activated IL-6 signaling pathway in the liver.

cGKI in the brain does not interact with hepatic insulin signaling and energy metabolism. To dissect whether the described phenotypes are related to cGKI in the brain, we compared glucose metabolism, as well as insulin and IL-6 signaling of conditional cGKI-BKO mice, which lack cGKI in the brain, with controls. cGKI-BKO mice displayed normal fasting blood glucose levels (Fig. 7*A*), glucose tolerance (Fig. 7*B*), and insulin tolerance (Fig. 7*C*). In contrast with cGKI-SM mice, basal and insulin-induced IR phosphorylation in the liver (Fig. 7*D*), serum IL-6 (Fig. 7*E*), and hepatic SOCS-3 mRNA and protein levels (Fig. 7*F*) were not altered. Moreover, cGKI-BKO mice had a normal body weight (Fig. 7*G*), locomotor activity (Fig. 7*H*), and energy expenditure (Fig. 7*I*). These results suggested that the cGMP/cGKI pathway in the brain does not interfere with insulin action in the liver and energy metabolism.

Increased macrophage infiltration in the liver of cGKI-SM mice. To further analyze the mechanism of liver inflammation and impaired hepatic insulin signaling in cGKI-SM mice, the cellular makeup of their livers was compared with control mice. As shown in Fig. 8*A*, the relative amount of CRBP-I–positive hepatic stellate cells, which coexpress cGKI in wild-type mice (Fig. 1*B*), was not altered in the absence of cGKI. However, the fraction of Mac-2–positive macrophages was significantly elevated in the liver of cGKI-SM mice (Fig. 8*B*). Because cGKI is not expressed in Mac-2–positive liver macrophages of wild-type mice (Fig. 1*B*), these results suggested that cGKI in hepatic stellate cells enhances macrophage infiltration via

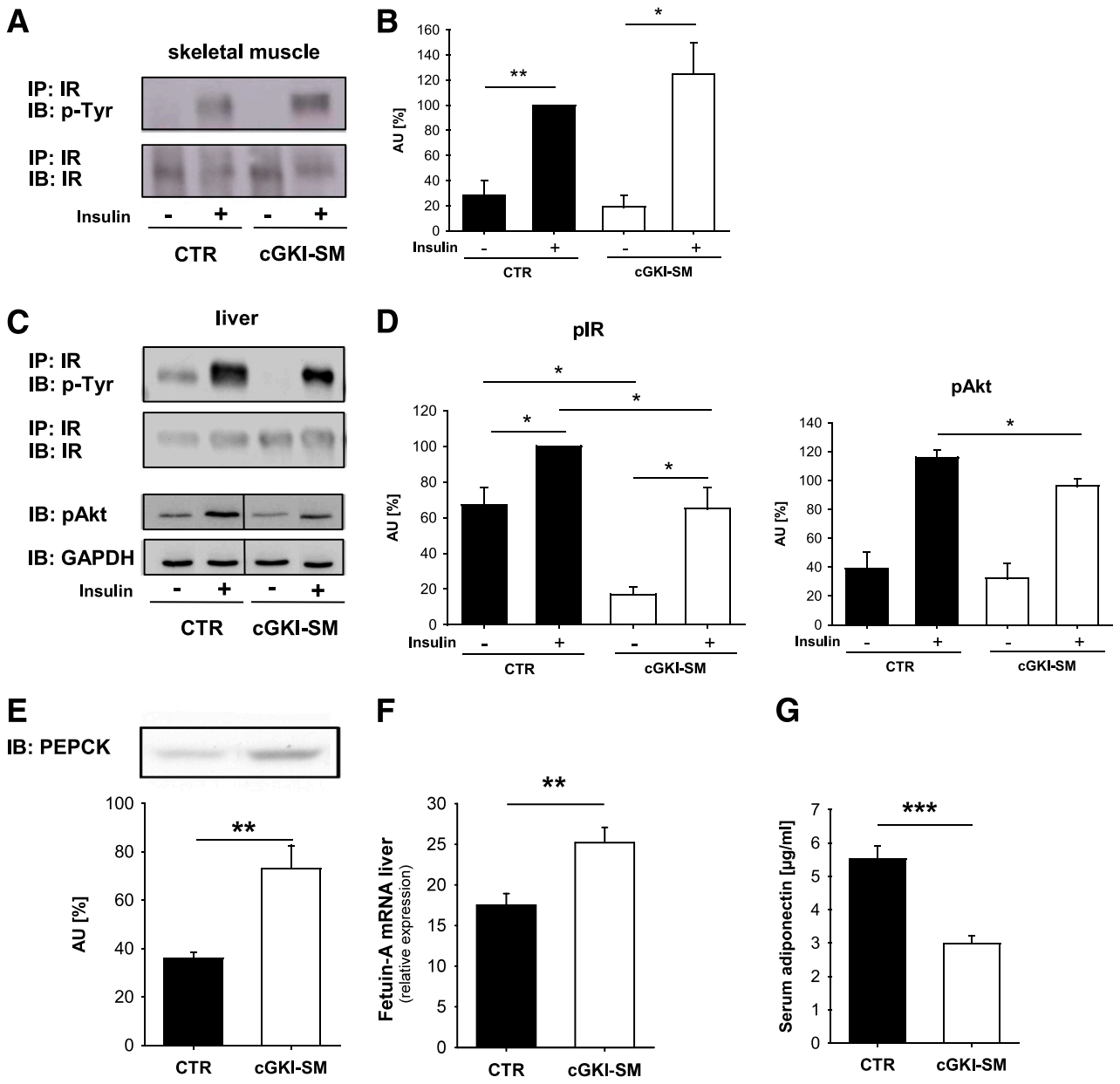

FIG. 5. Insulin signaling in skeletal muscle (*A* and *B*) and liver (*C* and *D*) of cGKI-SM (open bars) and control (black bars) mice. Mice received an intravenous injection of 2 units of human insulin or vehicle. Tyrosine phosphorylation of the IR was detected in immunoprecipitates of the IR (IP: IR) by immunoblotting with a phospho-tyrosine specific antibody (IB: *p*-Tyr; *upper blots*). The total level of IR was used as a loading control (IB: IR; *lower blots*). *A*: Tyrosine phosphorylation of the IR in skeletal muscle. The shown immunoblot is representative of three independent experiments. *B*: Densitometric analysis of the fraction of tyrosine phosphorylated IR in skeletal muscle. Results are given in arbitrary units (AU) (n = 3 mice per group). *C*: Tyrosine phosphorylation of the IR (*upper*) and phosphorylation of Akt at Ser473 (*lower*) in the liver; as loading controls, IR and GAPDH were used, respectively. The immunoblots shown are representative of three to four independent experiments. *D*: Densitometric analysis of the fraction of tyrosine phosphorylated IR (n = 3 mice per group) and phospho-Akt (Ser473) (n = 5–7 mice) in the liver. Results are given in AU. *E*: Western blot analysis of PEPCK expression in the liver after fasting and refeeding. The shown immunoblot is representative of one experiment with six control and five cGKI-SM mice. The results of the densitometric analysis are given in AU. *F*: Expression analysis of hepatic fetuin-A mRNA by quantitative RT-PCR (n = 4–6 mice per group). *G*: Fasting serum adiponectin levels (n = 11 mice per group). CTR, control. (A high-quality color representation of this figure is available in the online issue.)

a paracrine mechanism. The mechanism likely involves cytokines including IL-6 that result in increased liver inflammation and impaired insulin action.

DISCUSSION

Our data suggest that deletion of the cGKI in hepatic stellate cells results in enhanced recruitment of IL-6–secreting macrophages to the liver, thereby inhibiting insulin signaling. Extensive work has shown that IR signaling can be attenuated at the level of IR substrate (Irs) proteins by several serine kinases that are activated by obesity and inflammation, such as JNK, IKK, S6K1, and PKCs (29–32). NO/cGMP signaling has also been implicated in the modulation of glucose homeostasis, and the serine/threonine protein kinase cGKI is an important effector of this pathway (1–4). cGKI is highly expressed in smooth muscle cells, where it plays a crucial role in relaxation (10,20,33) and in several brain regions (16). This study elucidated the role of cGKI in glucose metabolism in vivo and focused

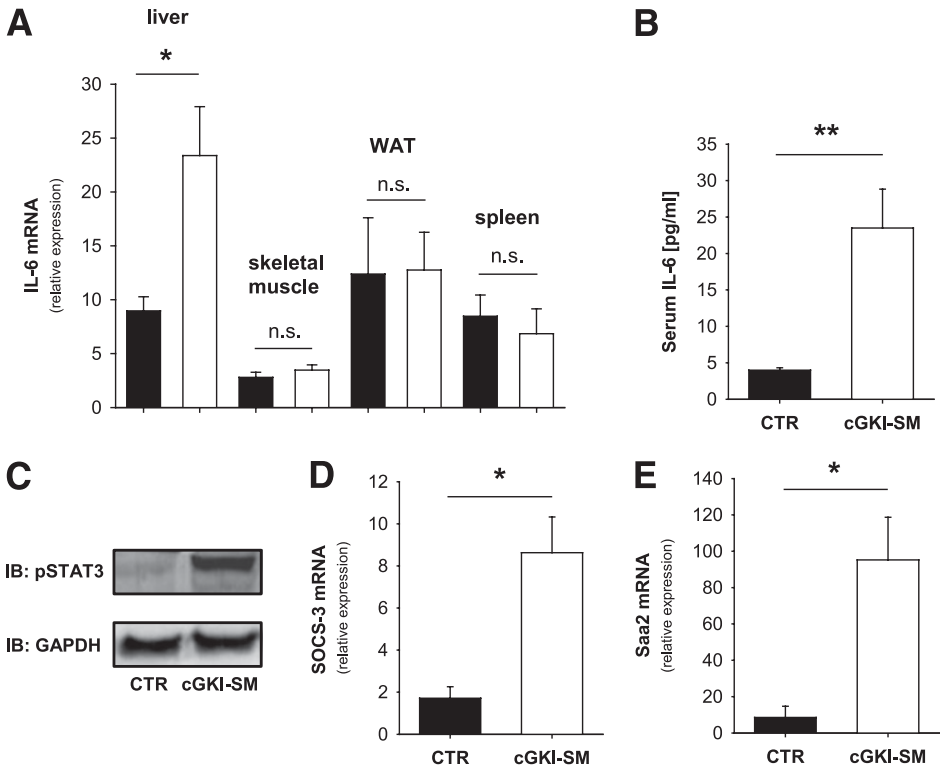

FIG. 6. IL-6 signaling in cGKI-SM (open bars) and control (black bars) mice. *A*: Expression analysis of IL-6 mRNA in various tissues by quantitative RT-PCR (n = 4–6 mice per group). *B*: Serum IL-6 concentrations (n = 7–8 mice per group). *C*: Phosphorylation of hepatic STAT3. Liver tissue was analyzed by immunoblotting with a phospho-STAT3 (Tyr705) antibody. GAPDH was used as a loading control. One representative immunoblot of three independent experiments with 8–10 mice is shown. Expression analysis of SOCS-3 mRNA (*D*) and serum amyloid A2 mRNA (*E*) by quantitative RT-PCR (n = 4–6 mice per group). CTR, control. WAT, white adipose tissue.

on potential interactions between cGMP/cGKI and insulin action. We report that cGKI-SM mice, which are deficient for endogenous cGKI in all tissues except smooth muscle, show a complex metabolic phenotype associated with liver inflammation and fasting hyperglycemia. This phenotype was not observed in neuron-specific cGKI knockout mice demonstrating that it was not due to a defect of cGMP/cGKI signaling in the brain. It is also unlikely that the defects reflect a role of cGKI in fat cells, skeletal muscle, pancreatic β-cells, or kidney epithelial cells, because we were unable to detect cGKI protein in these cell types in wild-type mice. In the liver, cGKI was undetectable in hepatocytes, but expressed in CRBP-I–positive stellate cells. To our knowledge, this is the first report of cGKI expression in hepatic stellate cells. The cGKI might be a potential downstream mediator of cGMP signaling in these cells. Indeed, previous studies have already indicated the presence of cGMP-generating enzymes in hepatic stellate cells (34).

The current study shows that cGKI-SM mice have higher energy expenditure in the light phase than control mice. The higher metabolic rate could, at least in part, explain their reduced fat mass and improved whole-body insulin sensitivity. It is unlikely that these phenotypes are linked to a defective central regulation, because cGKI-BKO mice showed normal energy expenditure, body weight, and insulin sensitivity. On the basis of the expression profile of cGKI, a direct interaction between cGKI and insulin action in fat cells or skeletal muscle seems unlikely. Moreover, insulin-stimulated tyrosine phosphorylation of the IR was not significantly altered in skeletal muscle of cGKI mutant mice. Therefore, we hypothesize that the improved whole-body insulin sensitivity of cGKI-SM mice is related to their higher energy expenditure and slightly reduced body weight and fat content with similar food intake. On the other hand, cGKI-SM mice had normal basal and glucose-stimulated insulin levels, and their glucose tolerance was indistinguishable from that of control mice. These data, together with the lack of cGKI expression in β-cells of wild-type mice, indicate that the cGMP/cGKI pathway is not involved in insulin secretion. This result does not contradict previous studies that suggested a role of NO or cGMP in insulin-secreting cells (1,2) because both NO and cGMP can exert effects independently of cGKI. cGKI-SM mice displayed profound fasting hyperglycemia but normal insulin levels. Although recent work suggests an involvement of cGKI in the secretion of glucagon (35), our expression analyses do not support a direct role of cGKI in glucagon-secreting α-cells (data not shown). Basal and insulin-stimulated IR tyrosine phosphorylation was significantly reduced in the liver of cGKI-SM mice, and in line with this, insulin-induced Akt phosphorylation at Ser473 was decreased as well. Together with elevated expression of PEPCK after fasting and refeeding, these findings indicate impaired hepatic insulin action in cGKI-SM mice.

Chronic inflammation is one of the major factors causing hepatic insulin resistance, and the cytokine IL-6 is known to play a key role. Elevated IL-6 levels cause hepatic insulin resistance both in vitro (36,37) and in vivo (24,38). IL-6–induced insulin resistance is mediated, at least in part, by tyrosine phosphorylation and activation of the transcription factor STAT3, resulting in stimulation of

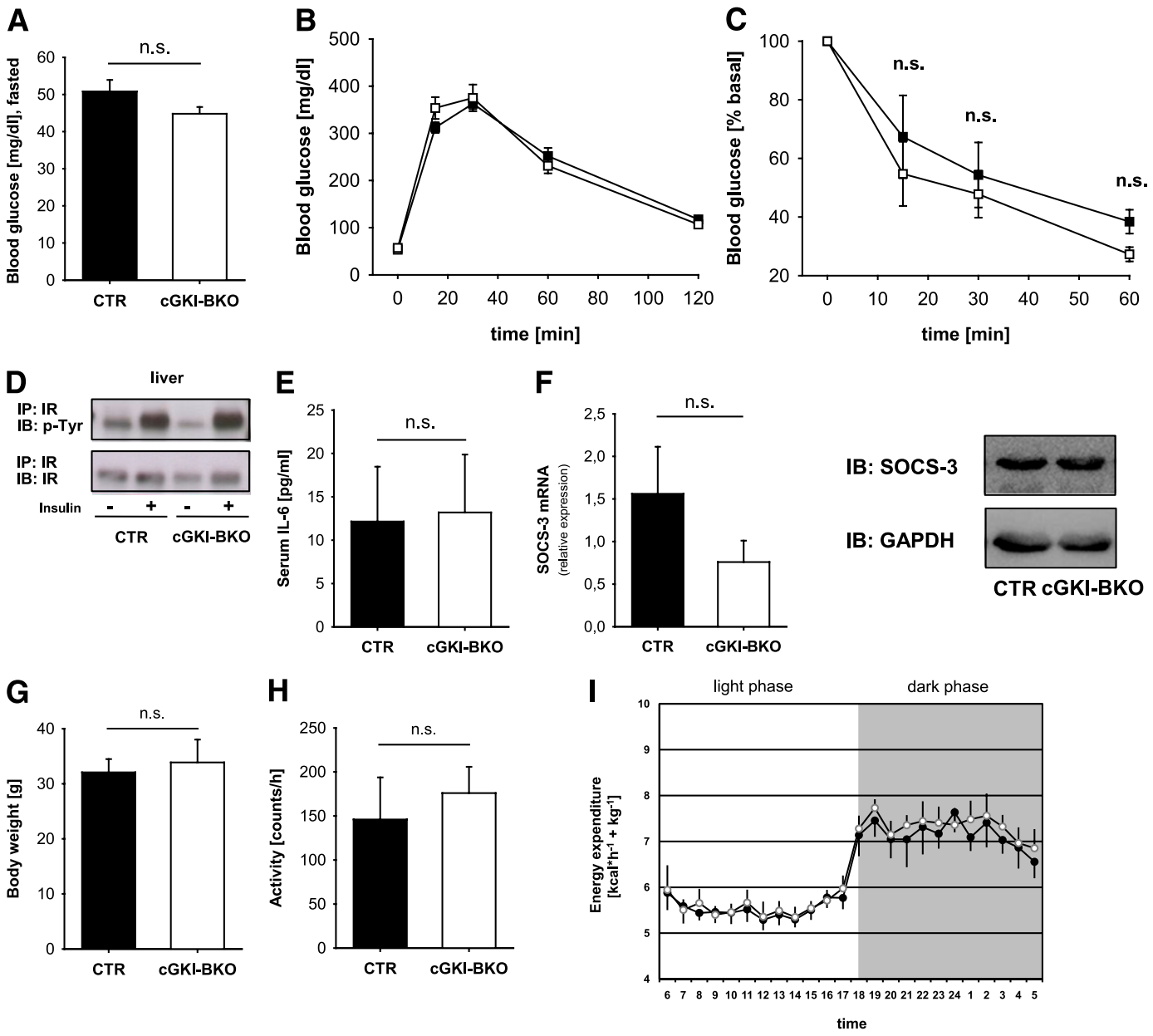

FIG. 7. Analysis of neuron-specific cGKI knockout mice (cGKI-BKO mice, open bars and symbols) and their litter-matched controls (black bars and symbols). *A*: Blood glucose concentrations were measured in tail blood of overnight fasted mice (n = 5 per group). *B*: Glucose tolerance tests were performed in overnight fasted mice as described in RESEARCH DESIGN AND METHODS and in the Fig. 4 legend (n = 5–6 mice per group). *C*: Insulin tolerance tests were performed in fed mice after intraperitoneal loading with 0.75 units of human insulin per kg body wt. Tail blood samples were taken at the indicated time points, and glucose was determined (n = 4 mice per group). *D*: Tyrosine phosphorylation of the IR in the liver was determined as described in the Fig. 5 legend. Shown are representative immunoblots of three independent experiments. *E*: Serum IL-6 concentrations (n = 5 mice per group). *F*: SOCS-3 mRNA expression in the liver (n = 5 mice per group) and protein levels (one representative immunoblot is shown, n = 4). Body weight (*G*), general locomotor activity (*H*), and total energy expenditure (*I*) were monitored over 24 h in cGKI-BKO mice (n = 5) and control mice (n = 5) as described in RESEARCH DESIGN AND METHODS and in the Fig. 3 legend. Mice in *A–F* were 5 months old, and mice in *G–I* were 9 to 12 months old. CTR, control. (A high-quality color representation of this figure is available in the online issue.)

SOCS-3 expression (27). SOCS-3 downregulates insulin action via several mechanisms, such as binding to the IR (39), inhibition of tyrosine phosphorylation of Irs1 and Irs2 (37), or reduction of Irs1 and Irs2 protein levels by stimulation of their proteosome-mediated degradation (40). Indeed, cGKI-SM mice had significantly elevated IL-6 levels in their liver and circulation. Moreover, the IL-6 signaling cascade was strongly activated in the liver of cGKI-SM mice as monitored by enhanced phosphorylation of STAT3 at tyrosine 705 and increased expression of SOCS-3 and serum amyloid A2. Serum IL-6 levels in the mutant mice were approximately sixfold higher than those present in healthy humans but similar to those seen in different states of chronic inflammation (41,42).

It is important to note that IL-6 mRNA was elevated in the liver of cGKI-SM mice but not in skeletal muscle, white adipose tissue, and spleen. Thus, the liver might be the primary source for increased circulating IL-6. In wild-type mice, cGKI is expressed in hepatic stellate cells but not in hepatocytes and other liver cells. How could loss of cGKI in stellate cells lead to increased hepatic IL-6? It is well known that stellate cells have a remarkable plasticity

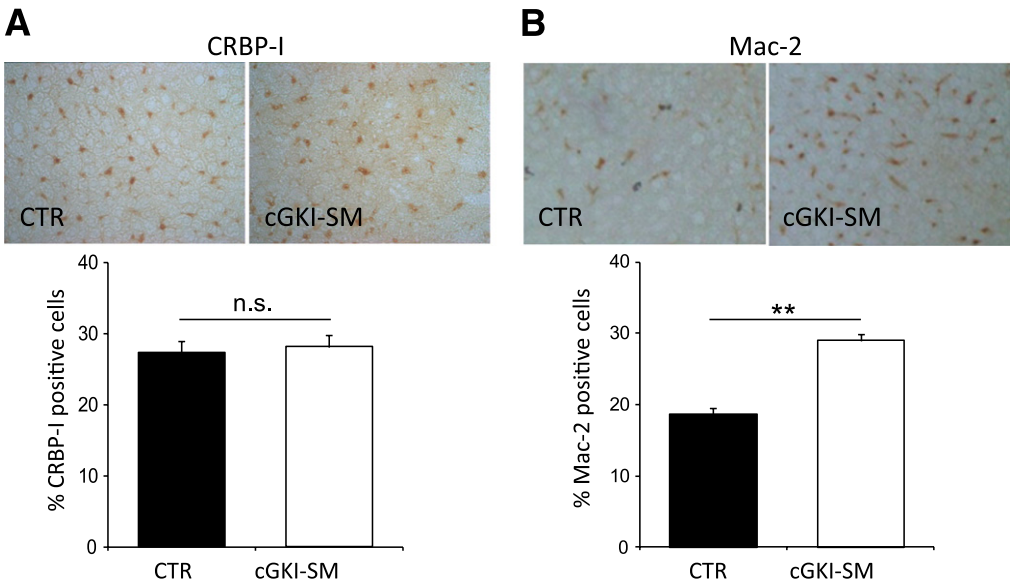

FIG. 8. Quantification of CRBP-I–positive cells (*A*) and Mac-2–positive cells (*B*) in the liver of cGKI-SM (open bars) and control (black bars) mice. Liver sections were stained with antibodies against CRBP-I or Mac-2. Original magnification was 40×. *Upper panels* show photomicrographs representative of four stained sections that were derived from four mice (one section per mouse). *Lower panels* show the fraction of positive cells (brown). Cells were counted in three microscopic fields of one section per mouse as described in RESEARCH DESIGN AND METHODS (n = 4 mice per group). CTR, control. (A high-quality digital representation of this figure is available in the online issue.)

and are crucial for the control of liver homeostasis via paracrine interactions with other resident liver cells (34). In particular, stellate cells secrete and respond to a number of cytokines, including IL-6. Dysfunction of the cGMP/cGKI pathway in stellate cells was associated with a markedly increased fraction of Mac-2–positive macrophages in the liver, without affecting the number of stellate cells. Thus, although increased IL-6 secretion by cGKI-deficient stellate cells cannot be excluded, it is likely that enhanced macrophage infiltration and macrophage-derived IL-6 play a major role for liver inflammation and insulin resistance in cGKI-SM mice. Stellate cells produce factors that regulate macrophage accumulation and growth, such as monocyte chemoattractant protein-1 (34). Although we could not detect altered expression of monocyte chemoattractant protein-1 mRNA in livers of cGKI-SM mice (Supplementary Fig. 1*D*), serum granulocyte colony-stimulating factor was clearly elevated in these mice, i.e., two of two IL-6–positive cGKI-SM mice were positive for granulocyte colony-stimulating factor (data not shown). Further experiments are needed to dissect the autocrine/paracrine mechanisms of this novel hepatic cGMP/cGKI pathway in more detail.

On the basis of our results, alternative mechanisms could also contribute to hepatic inflammation and impaired IR phosphorylation in cGKI-SM mice. The liver protein fetuin-A acts as a natural inhibitor of the IR tyrosine kinase (43–45), induces IL-6 expression, and suppresses the production of the insulin-sensitizing adipokine, adiponectin (21,46,47). Indeed, expression of fetuin-A mRNA was elevated in the liver of cGKI-SM mice, whereas circulating adiponectin levels were significantly repressed.

The elevated IL-6 level might not only affect liver metabolism but also contribute to the development of other phenotypes that are observed in cGKI-SM mice. In addition to a lipolytic effect of IL-6 in adipose tissues (48), several studies reported an antiobesity effect of low doses of IL-6 at the level of the brain, leading to increased energy expenditure and decreased body weight (29). Moreover, administration of IL-6 to human volunteers induced higher energy expenditure (49) and elevated fasting blood glucose levels (50). Macrophage-derived IL-6 may also cause anemia via induction of the iron-regulatory hormone hepcidin in hepatocytes (51). Thus, elevated IL-6 in cGKI-SM mice may, at least in part, be responsible for their increased energy expenditure, lean phenotype, fasting hyperglycemia, and anemia (22).

In conclusion, this study provides evidence that the cGMP/cGKI pathway does not directly interfere with the insulin signaling cascade in skeletal muscle, β-cells, and the brain. However, adequate liver metabolism depends on cGKI action because loss of this protein kinase results in hepatic inflammation. This phenotype might, at least in part, be caused by increased IL-6 signaling. We propose that loss of cGKI in hepatic stellate cells stimulates macrophage infiltration and activation of the hepatic IL-6/STAT3/SOCS-3 pathway, which leads to impaired insulin action and fasting hyperglycemia.

ACKNOWLEDGMENTS

This study was supported by the Deutsche Forschungsgemeinschaft (HE 3653/3-1, FE 438/2-1), the German Federal Ministry of Education and Research (DLR01GI0925), and the fortüne-Programm der Medizinischen Fakultät der Universität Tübingen (grant 1774-0-0).

No potential conflicts of interest relevant to this article were reported.

S.Z.L. wrote the article and researched data. A.M.H. reviewed the article and researched data. S.F. researched data and contributed to discussion. A.P. researched data. A.G. researched data and contributed to discussion. J.M., S.M.K., M.R., and A.S. researched data. C.W. researched data and contributed to discussion. H.-U.H. reviewed the article and contributed to discussion. R.F. reviewed and wrote the article.

The authors thank R. Lammers (Department of Internal Medicine IV, University of Tübingen, Germany) for providing the anti-IR antibody; E. Metzinger, D. Neuscheler, and H. Runge (all Department of Internal Medicine IV, University of Tübingen, Germany), and B. Birk (Interfakultäres Institut für Biochemie, University of Tübingen, Germany), who were involved in analytic procedures; K. Kantartzis and N. Stefan (both Department of Internal Medicine IV, University of Tübingen, Germany) for helpful instructions; R. Klein (Max Planck Institute of Neurobiology, Department of Molecular Neurobiology, Martinsried, Germany) for the Nes-Cre mouse line; and Miriam Hoene (Department of Internal Medicine IV, University of Tübingen, Germany) for glycogen measurements.

REFERENCES

1. Smukler SR, Tang L, Wheeler MB, Salapatek AM. Exogenous nitric oxide and endogenous glucose-stimulated beta-cell nitric oxide augment insulin release. Diabetes 2002;51:3450–3460
2. Kaneko Y, Ishikawa T, Amano S, Nakayama K. Dual effect of nitric oxide on cytosolic Ca2+ concentration and insulin secretion in rat pancreatic beta-cells. Am J Physiol Cell Physiol 2003;284:C1215–C1222
3. Francis SH, Corbin JD. Cyclic nucleotide-dependent protein kinases: intracellular receptors for cAMP and cGMP action. Crit Rev Clin Lab Sci 1999;36:275–328
4. Pfeifer A, Ruth P, Dostmann W, Sausbier M, Klatt P, Hofmann F. Structure and function of cGMP-dependent protein kinases. Rev Physiol Biochem Pharmacol 1999;135:105–149
5. Schlossmann J, Feil R, Hofmann F. Insights into cGMP signalling derived from cGMP kinase knockout mice. Front Biosci 2005;10:1279–1289
6. Feil R, Lohmann SM, de Jonge H, Walter U, Hofmann F. Cyclic GMP-dependent protein kinases and the cardiovascular system: insights from genetically modified mice. Circ Res 2003;93:907–916
7. Feil R, Hofmann F, Kleppisch T. Function of cGMP-dependent protein kinases in the nervous system. Rev Neurosci 2005;16:23–41
8. Kaminski A, Gao H, Morgan NG. Involvement of the cGMP signalling pathway in the regulation of viability in insulin-secreting BRIN-BD11 cells. FEBS Lett 2004;559:118–124
9. Miyashita K, Itoh H, Tsujimoto H, et al. Natriuretic peptides/cGMP/cGMP-dependent protein kinase cascades promote muscle mitochondrial biogenesis and prevent obesity. Diabetes 2009;58:2880–2892
10. Weber S, Bernhard D, Lukowski R, et al. Rescue of cGMP kinase I knockout mice by smooth muscle specific expression of either isozyme. Circ Res 2007;101:1096–1103
11. Langmesser S, Franken P, Feil S, Emmenegger Y, Albrecht U, Feil R. cGMP-dependent protein kinase type I is implicated in the regulation of the timing and quality of sleep and wakefulness. PLoS ONE 2009;4:e4238
12. Valtcheva N, Nestorov P, Beck A, et al. The commonly used cGMP-dependent protein kinase type I (cGKI) inhibitor Rp-8-Br-PET-cGMPS can activate cGKI in vitro and in intact cells. J Biol Chem 2009;284:556–562
13. Wegener JW, Nawrath H, Wolfsgruber W, et al. cGMP-dependent protein kinase I mediates the negative inotropic effect of cGMP in the murine myocardium. Circ Res 2002;90:18–20
14. Machann J, Thamer C, Schnoedt B, et al. Standardized assessment of whole body adipose tissue topography by MRI. J Magn Reson Imaging 2005;21:455–462
15. Buchmann J, Meyer C, Neschen S, et al. Ablation of the cholesterol transporter adenosine triphosphate-binding cassette transporter G1 reduces adipose cell size and protects against diet-induced obesity. Endocrinology 2007;148:1561–1573
16. Feil S, Zimmermann P, Knorn A, et al. Distribution of cGMP-dependent protein kinase type I and its isoforms in the mouse brain and retina. Neuroscience 2005;135:863–868
17. Plum L, Belgardt BF, Brüning JC. Central insulin action in energy and glucose homeostasis. J Clin Invest 2006;116:1761–1766
18. Van Rossen E, Vander Borght S, van Grunsven LA, et al. Vinculin and cellular retinol-binding protein-1 are markers for quiescent and activated hepatic stellate cells in formalin-fixed paraffin embedded human liver. Histochem Cell Biol 2009;131:313–325
19. Patsouris D, Li PP, Thapar D, Chapman J, Olefsky JM, Neels JG. Ablation of CD11c-positive cells normalizes insulin sensitivity in obese insulin resistant animals. Cell Metab 2008;8:301–309
20. Pfeifer A, Klatt P, Massberg S, et al. Defective smooth muscle regulation in cGMP kinase I-deficient mice. EMBO J 1998;17:3045–3051
21. Hennige AM, Staiger H, Wicke C, et al. Fetuin-A induces cytokine expression and suppresses adiponectin production. PLoS One 2008;3:e1765
22. Föller M, Feil S, Ghoreschi K, et al. Anemia and splenomegaly in cGKI-deficient mice. Proc Natl Acad Sci U S A 2008;105:6771–6776
23. Inoue H, Ogawa W, Asakawa A, et al. Role of hepatic STAT3 in brain-insulin action on hepatic glucose production. Cell Metab 2006;3:267–275
24. Klover PJ, Zimmers TA, Koniaris LG, Mooney RA. Chronic exposure to interleukin-6 causes hepatic insulin resistance in mice. Diabetes 2003;52:2784–2789
25. Kim HJ, Higashimori T, Park SY, et al. Differential effects of interleukin-6 and -10 on skeletal muscle and liver insulin action in vivo. Diabetes 2004;53:1060–1067
26. Klover PJ, Clementi AH, Mooney RA. Interleukin-6 depletion selectively improves hepatic insulin action in obesity. Endocrinology 2005;146:3417–3427
27. Torisu T, Sato N, Yoshiga D, et al. The dual function of hepatic SOCS3 in insulin resistance in vivo. Genes Cells 2007;12:143–154
28. Klein C, Wüstefeld T, Assmus U, et al. The IL-6-gp130-STAT3 pathway in hepatocytes triggers liver protection in T cell-mediated liver injury. J Clin Invest 2005;115:860–869
29. Wellen KE, Hotamisligil GS. Inflammation, stress, and diabetes. J Clin Invest 2005;115:1111–1119
30. Taniguchi CM, Emanuelli B, Kahn CR. Critical nodes in signalling pathways: insights into insulin action. Nat Rev Mol Cell Biol 2006;7:85–96
31. Aguirre V, Uchida T, Yenush L, Davis R, White MF. The c-Jun NH(2)-terminal kinase promotes insulin resistance during association with insulin receptor substrate-1 and phosphorylation of Ser(307). J Biol Chem 2000;275:9047–9054
32. Paz K, Hemi R, LeRoith D, et al. A molecular basis for insulin resistance. Elevated serine/threonine phosphorylation of IRS-1 and IRS-2 inhibits their binding to the juxtamembrane region of the insulin receptor and impairs their ability to undergo insulin-induced tyrosine phosphorylation. J Biol Chem 1997;272:29911–29918
33. Feil R, Gappa N, Rutz M, et al. Functional reconstitution of vascular smooth muscle cells with cGMP-dependent protein kinase I isoforms. Circ Res 2002;90:1080–1086
34. Friedman SL. Hepatic stellate cells: protean, multifunctional, and enigmatic cells of the liver. Physiol Rev 2008;88:125–172
35. Leiss V, Friebe A, Welling A, Hofmann F, Lukowski R. Cyclic GMP kinase I modulates glucagon release from pancreatic α-cells. Diabetes 2011;60:148–156
36. Senn JJ, Klover PJ, Nowak IA, Mooney RA. Interleukin-6 induces cellular insulin resistance in hepatocytes. Diabetes 2002;51:3391–3399
37. Senn JJ, Klover PJ, Nowak IA, et al. Suppressor of cytokine signaling-3 (SOCS-3), a potential mediator of interleukin-6-dependent insulin resistance in hepatocytes. J Biol Chem 2003;278:13740–13746
38. Sabio G, Das M, Mora A, et al. A stress signaling pathway in adipose tissue regulates hepatic insulin resistance. Science 2008;322:1539–1543
39. Emanuelli B, Peraldi P, Filloux C, Sawka-Verhelle D, Hilton D, Van Obberghen E. SOCS-3 is an insulin-induced negative regulator of insulin signaling. J Biol Chem 2000;275:15985–15991
40. Rui L, Yuan M, Frantz D, Shoelson S, White MF. SOCS-1 and SOCS-3 block insulin signaling by ubiquitin-mediated degradation of IRS1 and IRS2. J Biol Chem 2002;277:42394–42398
41. Eder K, Baffy N, Falus A, Fulop AK. The major inflammatory mediator interleukin-6 and obesity. Inflamm Res 2009;58:727–736
42. Preti HA, Cabanillas F, Talpaz M, Tucker SL, Seymour JF, Kurzrock R. Prognostic value of serum interleukin-6 in diffuse large-cell lymphoma. Ann Intern Med 1997;127:186–194
43. Auberger P, Falquerho L, Contreres JO, et al. Characterization of a natural inhibitor of the insulin receptor tyrosine kinase: cDNA cloning, purification, and anti-mitogenic activity. Cell 1989;58:631–640
44. Rauth G, Pöschke O, Fink E, et al. The nucleotide and partial amino acid sequences of rat fetuin. Identity with the natural tyrosine kinase inhibitor of the rat insulin receptor. Eur J Biochem 1992;204:523–529
45. Srinivas PR, Wagner AS, Reddy LV, et al. Serum alpha 2-HS-glycoprotein is an inhibitor of the human insulin receptor at the tyrosine kinase level. Mol Endocrinol 1993;7:1445–1455
46. Stefan N, Hennige AM, Staiger H, et al. Alpha2-Heremans-Schmid glycoprotein/fetuin-A is associated with insulin resistance and fat accumulation in the liver in humans. Diabetes Care 2006;29:853–857
47. Mori K, Emoto M, Yokoyama H, et al. Association of serum fetuin-A with insulin resistance in type 2 diabetic and nondiabetic subjects. Diabetes Care 2006;29:468
48. Watt MJ, Carey AL, Wolsk-Petersen E, Kraemer FB, Pedersen BK, Febbraio MA. Hormone-sensitive lipase is reduced in the adipose tissue of

patients with type 2 diabetes mellitus: influence of IL-6 infusion. Diabetologia 2005;48:105–112
49. Tsigos C, Papanicolaou DA, Defensor R, Mitsiadis CS, Kyrou I, Chrousos GP. Dose effects of recombinant human interleukin-6 on pituitary hormone secretion and energy expenditure. Neuroendocrinology 1997;66:54–62
50. Tsigos C, Papanicolaou DA, Kyrou I, Defensor R, Mitsiadis CS, Chrousos GP. Dose-dependent effects of recombinant human interleukin-6 on glucose regulation. J Clin Endocrinol Metab 1997;82:4167–4170
51. Nemeth E, Rivera S, Gabayan V, et al. IL-6 mediates hypoferremia of inflammation by inducing the synthesis of the iron regulatory hormone hepcidin. J Clin Invest 2004;113:1271–1276